The implementation of tactile feedback using squeeze film effect devices

Mélisande Biet, Frédéric Giraud, Betty Lemaire-Semail

EPJ manuscript No.
(will be inserted by the editor)

The implementation of tactile feedback using squeeze film effect devices

Mélisande Biet, Frédéric Giraud, and Betty Lemaire-Semail

Laboratoire d'Electrotechnique et d'Electronique de Puissance de Lille (L2EP)
Project ALCOVE-INRIA IRCICA
Polytech'Lille - Bt E
Avenue Paul Langevin
59655 Villeneuve d'Ascq, France
e-mail: melisande.biet@polytech-lille.fr

the date of receipt and acceptance should be inserted later

Abstract. This paper describes the implementation and initial evaluation of active-type tactile displays in desktop environments. The first device comprises a stator of an ultrasonic motor supplied by only one channel. In this way, the motor twisted of its application do not induce movement but can create slipperiness on the stator's surface. This effect can be interpreted as squeeze film phenomenon and allow us to change indirectly the friction on the surface and to generate shear forces on the fingertip, which in turn creates interesting tactile effects. Moreover, if we add a position sensor, we can vary the signal spatially which gives the sensation of bumps/ridges. Then, based on the first device principle, another device is proposed in order to enable a free exploration of the surface following ergonomic requirements.

PACS. 85.50-n Piezoelectric devices – 77.65-j Piezoelectricity and electromechanical effects

1 Introduction

Artificial tactile feedback provides an under-utilized channel which can be used in virtual reality not only to augment the reality of computer graphics but also to gain information about the state of a device, the occurrence of an event, or its content.
In desktop environments, the most common approach to make tactile displays is to pack a dense array of actuated pins (an early example of which can be found in [1]) and make them move orthogonally to the skin to approximate a texture. However, to simulate finely textured surface (surface unevenness scale is around $100\mu m$) and thus enhance tactile feedback reality, this kind of tactile device is not appropriated because there are some significant limitations including the difficulty of achieving a high density array, high power consumption, and high manufacturing cost. Due to these challenges, the resulting devices are typically complex or not portable.
Another possibility for simulating finely textured surfaces is the use of the squeeze film effect principle. It has been shown that a beam excited by ultrasonic vibration can give rise to a reduction of friction [2]. These squeeze bearings act as a cushion of air that lifts and separates the finger from the planar display surface. By varying the thickness of the squeeze bearing, the friction on the surface can be indirectly reduced. This device has the advantage of providing a continuous surface on the fingerpulp and avoids integration problems.
In this article, we first use this principle on the stator of an ultrasonic motor (part 2). After having verified that the squeeze film effect can occur on the stator ring, we add a position sensor and we modulate this effect by imposing low frequency periodic signal over the ultrasonic vibration. This allows us to show that we can vary the signal spatially and that we can give the sensation of bumps/ridges. However, even if this tactile device is more compact, has a lower weight and simulate more sensations comparatively to the Langevin's transducers used in [2], it is just a one degree-of-freedom (DOF) device and besides the finger movement is small.
Then, in order to solve this problem, we use a tactile plate able to generate the squeeze film effect (part 3). This plate can bend by means of PZT piezoceramics glued on one of the two surfaces. The monomorph built up in this manner can stimulate sensations similar to the previous ones but in this case in 2 directions.

2 A 1 DOF tactile display

The goal of this section is to present the 1 DOF tactile display and to assess if the slippiness feeling that we can feel is really due to the squeeze film effect. In order to show that, we calculate the pressure between the fingertip and the vibrating ring (stator). Afterwards, we modulate

the squeeze film effect by imposing low frequency periodic signals over the ultrasonic vibration and we qualitatively evaluate the sensation obtained.

2.1 Device

We propose to use a piezoelectric motor, the Shinsei USR 60 (Fig. 1a), to generate the slippery feeling under the fingerpulp. The test device is made of the stator, and the surface of this stator can be explored directly by users without any damage (Fig. 1b).
In normal working condition, the motor is supplied by two alternative phases which operates at the resonant frequency around 40 kHz. Each phase creates its own stationary wave around the stator, and the two stationary waves, in quadrature, create together a traveling one thanks to a right position of each phase ceramics and to their initial polarization.
Now, in our application, we just supply one channel so that a standing wave can appeared. In this way, the finger can not be dragged along of the stator and furthermore it is impossible to feel the traveling wave to come up if the finger is put on the vibrating stator . Nevertheless, we notice that we can add a smooth feeling to the stator's surface by applying standing wave ultrasonic vibration.
It may be remarked that the normal displacement of the

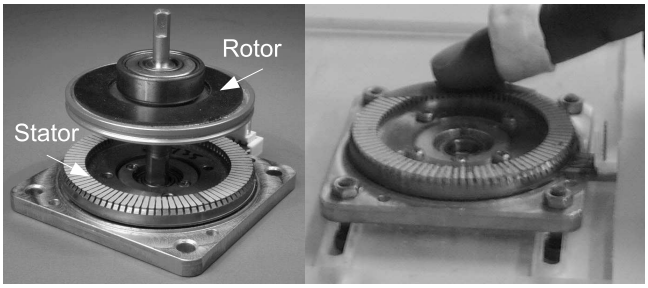

Fig. 1. a. The Piezo-electric motor(PEM) b. The stator of the PEM is the surface to touch.

rotor is too weak (a few μm) and that the vibration frequency is too high (40kHz) to be detected by the skin sensors [3]. For that reason, we suggest the possibility that the squeeze film effect could be the cause of the slippery feeling. Thus, in the next subsection we are going to verify this assumption.

2.2 Changing the relative friction coefficient with the squeeze film effect

2.2.1 Squeeze film model

In this subsection, we are describing the squeeze effect [4]. Indeed, we consider the gas film created between the fingertip and the vibrating stator (Fig. 2).

We are going to rely on a study developed in [5], but taking into account the fingerprints and the flexural mode

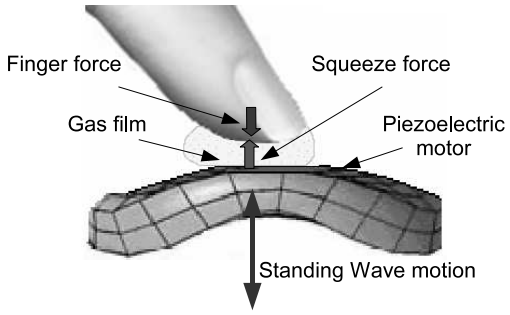

Fig. 2. Mechanism of slippage.

of the stator. In our case, we can not suppose that the undulations of the fingerprints are negligible relatively to the roughness of the vibrating plate (few micrometers) since the height (2he) and pitch (L) of the epidermal ridge are around 100 μm and 350 μm, respectively [6] (Fig.3).
Thus, we regard the tip of the finger as an undulated surface while the stator is assumed to bend sinusoidally in a vertical direction. The film thickness, h, is the sum of

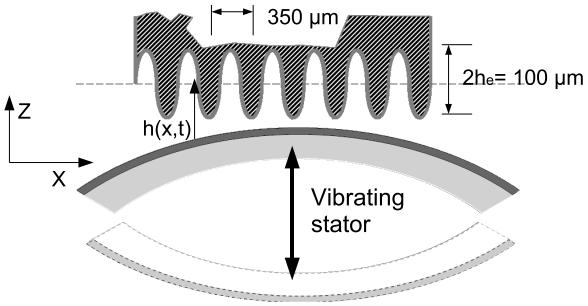

Fig. 3. Approximate profile of a fingertip on the vibrating stator when the epidermal ridges are taken into account.

the gap created when the finger skin cannot follow the ultrasonic vibration of the stator at all, which equals the amplitude of oscillation , h_{vib}, plus the surface unevenness (average roughness), h_r. h also considers the amplitude of the undulation of the fingerprint, h_e.

Therefore, the thickness of the film is given by [2]:

$$h(x,t) = (h_{vib}+h_r)[1+\cos(\omega_0 t)\cos(\frac{2\pi}{\lambda}x)]+h_e[1+\cos(\frac{2\pi}{L}x)] \quad (1)$$

In which $\omega_0/2\pi$ and λ are respectively the vibrating frequency and the wavelength of the piezoelectric motor (PEM). If we normalize h, the normalized airgap can be written with non dimensional parameters as:

$$H = 1 + \epsilon\cos(T)\cos(k_1 X) + \delta\cos(k_2 X) \quad (2)$$

with $h_0 = h_{vib} + h_r$, the non-dimensional parameters are

$$H = \frac{h}{h_0+h_e}, \quad X = \frac{x}{l_0}, \quad T = \omega_0 t,$$

$$\epsilon = \frac{h_0}{h_0+h_e}, \quad \delta = \frac{h_e}{h_0+h_e}, \quad k_1 = \frac{2\pi l_0}{\lambda}, \quad k_2 = \frac{2\pi l_0}{L}$$

where the length in contact with the fingertip is l_0.

We make the following assumptions [5]; 1) The fluid behavior is governed by laminar viscous flow, 2) The fluid is a compressible perfect gas, 3) The inertia effect of the flow is negligible, 4) The relative lateral motion is equal to zero. Under those conditions, the one-dimensional Navier-stock equation is obtained. This equation associated with continuity and ideal gas equations allows us to find the governing Reynolds equation in the non-dimensional form:

$$\nabla(H^3 P^{1/n}.\nabla(P)) = \sigma\frac{\partial(P^{1/n}H)}{\partial T} \tag{3}$$

In which n is a polytropic constant and where

$$P = \frac{p}{p_0}, \quad \sigma = \frac{12\eta\omega_0 l_0}{p_0(h_0+h_e)^2} \tag{4}$$

p, p_0 and η represent the pressure in the gap, the surrounding gas pressure and the dynamic viscosity of the fluid respectively. The squeeze number is given by σ, which represents a measurement of the fluid compressibility in the gap. At low squeeze numbers, the fluid is nearly incompressible, while at high squeeze numbers, the fluid is trapped in the gap and acts like a spring.

We further assume that the squeezed film is isothermal (n=1). The latter assumption is reasonable since the gas film is very thin and of low heat capacity when compared with that of the vibrating surfaces. Then, to simplify the time derivation term, we substitute PH by Ψ. For steady state conditions, the integration with respect to one period yields to [5]

$$\nabla[\frac{1}{2}\overline{H}\nabla(\Psi_\infty^2) - \Psi_\infty^2\nabla(\overline{H})] = 0 \tag{5}$$

where Ψ_∞ denotes the Ψ inside the airgap when $\sigma \to \infty$ and $\overline{H}$ is the mean normalized film thickness given by

$$\overline{H} = 1 + \delta\cos(k_2 X) \tag{6}$$

It may be noticed that the analytical solution is accurate as far as σ is assumed at a very large value. On the contrary, a low value of σ would imply a much more complex solution.

2.3 Approximate analytical solution

The equation 5 gives us the relationship between the normalized film thickness and the normalized pressure for a fluid behavior close to a spring. The solution of (5) is given by (Appendix A)[5]:

$$\Psi_\infty^2 = K_1[1+\delta\cos(k_2 X)]^2 \tag{7}$$

In which K_1 is a constant.
The boundary conditions with respect to $\Psi_\infty^2(X)$, noted down as $\Psi_{\infty B}$ are

$$\Psi_{\infty B}^2(-\frac{1}{2}) = \Psi_{\infty B}^2(\frac{1}{2}) = K_1[1+\delta\cos(\frac{k_2}{2})]^2 \tag{8}$$

In which $\frac{1}{2}$ is the normalized value of $\frac{l_0}{2}$.
By replacing K_1 by its expression in (7), we obtain:

$$\Psi_\infty = \Psi_{\infty B}(\frac{1}{2})\frac{|1+\delta\cos(k_2 X)|}{|1+\delta\cos(\frac{k_2}{2})|} \tag{9}$$

Furthermore, in order to find $\Psi_{\infty B}$, we will focus our attention on the boundary region. Considering that p_0 is constant in time and that $\Psi_{\infty B}$ equals Ψ_∞ when the boundary region meets the interior of the airgap, we obtain [5]:

$$\begin{aligned}\Psi_{\infty B}^2(\frac{1}{2}) &= p_0^2\frac{\int_T^{T+2\pi} H_B^3\,dT}{\int_T^{T+2\pi} H_B\,dT} \\ &= p_0^2\frac{\int_T^{T+2\pi}[1+\epsilon\cos(T)\cos(\frac{k_1}{2})+\delta\cos(\frac{k_2}{2})]^3\,dT}{\int_T^{T+2\pi}[1+\epsilon\cos(T)\cos(\frac{k_1}{2})+\delta\cos(\frac{k_2}{2})]\,dT} \\ &= p_0^2[1+\delta\cos(\frac{k_2}{2})]^2\left[1+\frac{3}{2}\frac{\epsilon^2}{[1+\delta\cos(\frac{k_2}{2})]^2}\right]\end{aligned} \tag{10}$$

By replacing $\Psi_{\infty B}$ by its expression in (9), we obtain:

$$\begin{aligned}P_\infty &= \frac{\Psi_\infty}{H} \\ &= p_0\frac{(1+\delta\cos(k_2 X))\sqrt{(1+\delta\cos(\frac{k_2}{2}))^2+\frac{3}{2}\epsilon^2\cos^2(\frac{k_1}{2})}}{(1+\delta\cos(\frac{k_2}{2}))(1+\epsilon\cos(T)\cos(\frac{k_1}{2})+\delta\cos(k_2 X))}\end{aligned} \tag{11}$$

Remember that P_∞ is the normalized pressure inside the airgap for an infinite value of the squeeze number σ. Then, the mean squeeze pressure is expressed by:

$$\overline{P_\infty} = p_0\frac{(1+\delta\cos(k_2 X))\sqrt{(1+\delta\cos(\frac{k_2}{2}))^2+\frac{3}{2}\epsilon^2\cos^2(\frac{k_1}{2})}}{(1+\delta\cos(\frac{k_2}{2}))\sqrt{(1+\delta\cos(k_2 X))^2-\epsilon^2\cos(\frac{k_1}{2})}} \tag{12}$$

2.3.1 Results

First of all, let us remind you that in order to predetermine analytically the over-pressure on the fingertip, we have to satisfy the following condition : $\sigma \to \infty$. However, we assume in practice that the squeeze pressure (P_∞) depends almost entirely on the amplitude of vibration when the squeeze number is larger than 10. Therefore, we calculate the squeeze number σ as shown in (4), with the parameters of Table 1. We obtain $\sigma = 20.4$ for $h_{vib} = 2\mu m$. This result enables us to use the equation (5) and to calculate the overpressure between the finger and the stator.

Using the parameters shown in Table.I, we can compute the pressure profile along the airgap using (Eq.11).

On the upper part of figure 4, the finger at contact is modeled as a sinusoid with an amplitude of $50\mu m$ in order to take into account the fingerprints. The interval from the zero depicts mean roughness plus the vibration amplitude of the vibrating plate itself. The curve below shows the evolution of the pressure temporal mean as a function of the position on X-axis. In this figure 4, pressure peaks are

Table 1. List of parameters

Amplitude of the fingerprint	h_e	50 $[\mu m]$
Period of the fingerprint	L	350 $[\mu m]$
Wavelength of the PEM	λ	18.7 $[mm]$
Resonance frequency of the PEM	$\frac{\omega_0}{2pi}$	40.5 $[kHz]$
Average roughness of the stator	h_r	0.6 $[\mu m]$
Length in contact	l_0	1 [cm]
Force applied by the fingertip	F_f	$0.3 \rightarrow 0.7$ [N]
Dynamic viscosity of air	η	$1.85.10^{-5}$[Pa.s]
Atmospheric pressure	p_0	0.1 [MPa]

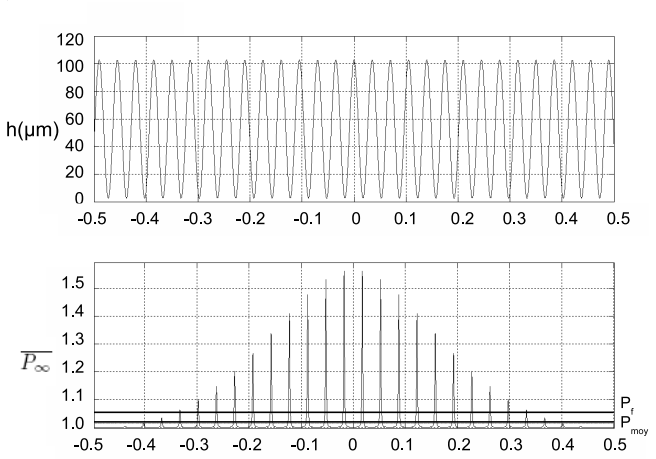

Fig. 4. Thickness of the film at a given time and spatial profile of the mean time pressure under the finger ($h_r = 0.6\mu m, h_{vib} = 2\mu m$)

localized where the finger-skin is as close as possible to the vibrating plate, i.e. at the fingerprint ridges, whereas at the fingerprint grooves, pressure is not far from the atmospheric pressure. The pressure P_f is the mean finger pressure that it is used during an exploration task.

$$P_f = F_f / l_0^2 \tag{13}$$

where F_f denotes the normal contact force applied by a person exploring the surface. For its value, we choose 0.5 N as a mean normal contact force according to [2][7].

We can notice from Fig. 4 that there are some zones of the fingerprint where the squeeze pressure is superior to the finger pressure. Those zones are not in contact with the vibrating plate. Moreover, the mean pressure P_{moy} (Fig. 4) is higher than 1, which means that the squeeze film effect is significant for ultrasonic frequency contact of the stator and the finger, as it has been previously shown for the stator and the rotor of the USR 60 [8].

Since the squeeze force occurs, we can express the relative coefficient of friction, $\frac{\mu'}{\mu}$ in terms of (Eq.14).

$$\frac{\mu'}{\mu} = 1 - \frac{(P_\infty - 1)}{P_f} \tag{14}$$

Physically, and following the assumptions previously defined, this equation means a weakening of the friction coefficient for a given surface when the squeeze force occurs.

To illustrate the friction coefficient variations, we can compute $\frac{\mu'}{\mu}$. The results are given in Fig.5.

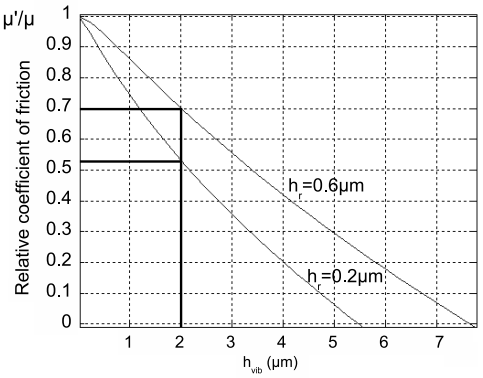

Fig. 5. The relative coefficient of friction as a function of the amplitude of vibration for $F_f = 0.5N$ and for $h_r = 0.2\mu m$ and $h_r = 0.6\mu m$.

We can easily calculate the relative friction coefficient, taking into account the fingerprints and the flexural mode of the stator. Moreover, those results show that surface roughness, contact area and the vibration amplitude are important parameters of the squeeze film effect. We have also to notice that the relative coefficient of friction is strongly dependent on the force applied by the user (F_f), thus the results of (Fig.5) have to be considered with care. The previous calculation is performed by assuming that the stator surface is flat and without teeth, which increase the contact area between the finger and the stator. However, owing to the ridge width is really larger than the groove width of the teeth, we assume that this choice has no important effect on the present study.
Furthermore, considering the Figure 5, a vibration amplitude of the stator higher than $7\mu m$ would be necessary to levitate the finger, i.e. to reach a zero relative friction coefficient. This value could appear very high but it is not necessary to reach it because a vibration amplitude of $2\mu m$ is enough to feel a difference of sensation.
Hence, by lubrication effect (squeeze film effect), we can succeed in changing the sensation by exploiting the friction coefficient between the finger and the plate as it was qualitatively checked in [9].

2.4 Space period variation for roughness simulation

2.4.1 Principle

Spatially varying voltage signals are effective at conveying a true sense of texture. Using position feedback (Fig. 6), it is fairly easy to make certain locations feel smoother than others. For that aim, we impose a periodic signal over the

standing wave at low frequency. This comes down to a disturbance injection or a wave amplitude modulation. As a result, the squeeze force is also modulated as well as the tangential speed. Thus, controlling the spatial frequency between slippery area leads to grooved textures because of the alternation between slippery and braking feeling. Many possibilities can be suggested following this principle: about the shape of the injected signals, about their frequency, and whether or not this frequency is tuned following the finger speed. For example we can use a square signal that turns off and on (pulse train), sine wave, localized pulses or velocity dependent signals.

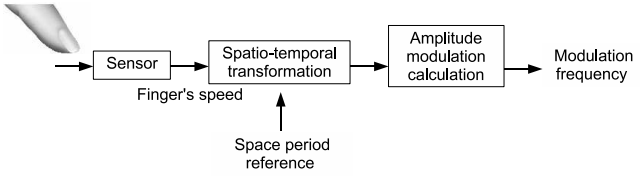

Fig. 6. Modulation of the squeeze film effect.

2.4.2 Experimental device

The experimental device is given in figure 7. As we need the finger speed and direction, a LVDT sensor is used. The connection to the finger is rigid in order to avoid some inconsistency in the behavior of all of the position based effects. Only linear displacements are allowed, which implied that the finger movement is quite small ($\approx 4cm$). Nevertheless, ahead or reverse motion may be done. The stator of the PEM is supply by only one channel so as to create a standing wave on the stator. Its maximum vibration amplitude measured with the LASER Doppler Vibrometer is $2\mu m$. Then, to add to the friction range, we apply a flat and braking adhesive on the surface of the stator ($h_r = 0.6\mu m$ instead of $0.2\mu m$ for the stator by itself [8]). According to Fig.5, the choice of the adhesive is crucial for a good working of the tactile device since the adhesive unevenness has a strong incidence on the squeeze film effect. The device is run in a real time environment

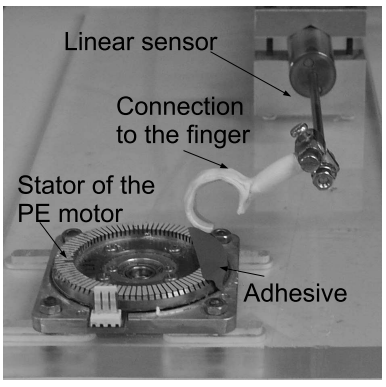

Fig. 7. The experimental device.

and textures are created in software as voltage patterns. In actual use, dragging with his finger, the user can feel the sensation of roughness thanks to a wave amplitude modulation. Moreover, textures with sharp changes in friction are much stronger than those with smooth transitions. For this reason, we use square pulses.

2.4.3 Evaluation of the device

If we change the space period, we can easily recognize whether the surface is finely or coarsely grooved. However, we need to evaluate this device to know if the space period we simulate correspond to the space period of a real gratings. Using a rectangular plate where several types of grooved surface are engraved, we carried out a match to sample experiment by comparing this plate and the 1 DOF device.

The experiment is conducted with twelve naive students aged between 18 and 25 years. Gratings are single sided copper printed circuit boards (PCBs). The PCBs measure 7 by 130mm and are etched with striated layouts as shown in figure 8. The copper thickness or height of ridge is equal to $70\mu m$. The groove width and the ridge width of the gratings are respectively equal to 0.4, 2, 4, 8 and 10mm. This gratings are hidden in a box so as to not be influenced by vision.

The subject's task is put his/her index finger in the sensor ring and to form a straight line on the stator surface with a backward and forward motion of his/her finger to discover the virtual surface. Then he/she has to compare his/her sensation with the gratings in the box (fig.9). To improve the match to sample procedure, gratings are first

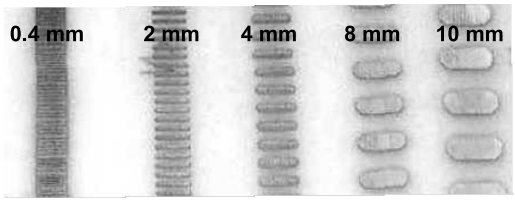

Fig. 8. Gratings used for the match to sample experiment.

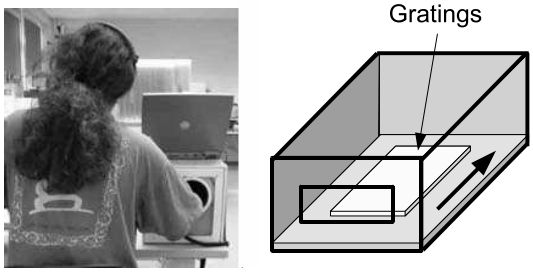

Fig. 9. Experimental Setup.

randomly presented to participants. After this preliminary phase, subjects has to evaluate the "virtual surface". They are asked to say which gratings looks like the "virtual surface" tested.

Space period of the gratings	**Space period simulated**				
	0.4 mm	2 mm	4 mm	8 mm	10 mm
0.4 mm					
2 mm					
4 mm					
8 mm					
10 mm					

Table 2. Percentage of answer

The test result is shown in Table. It can be seen from the results that users are able to distinguish the range of the spatial period. Difference of the displayed sensation was clear except for the last case (0.4 mm).

2.4.4 Limitations and improvements

This experiment is a preliminary evaluation, which shows that the 1 DOF tactile display can produce several distinct sensations. Effectively, several periodic rough textures can be simulated, with a low frequency wave modulation. The modulation signal has also to be tuned according to the fingers speed. However, even if this tactile device is more compact, has a lower weight and simulate more sensations comparatively to the Langevin's transducers used in [2], it is just a one degree-of-freedom (DOF) device and besides the finger movement is small. Thus, due to the small one-dimensional workspace of the 1 DOF tactile display, the range of texture sensations is consequently limited. A larger, two-dimensional array able to generate the squeeze film effect has to be designed in order to solve this problem. This new device should be able to improved the sensation and to generate new modes of texture with spatial signals that can vary in two dimensions.

The limitation concerns finger orientation. In the course of testing, we found that there was a significant difference in the intensity of the perceived texture depending on whether the finger touched the plates with a horizontal or vertical orientation. Thus, it is important that the user interacts with the device using a consistent finger orientation [10].

3 Roughness simulation on a 2 dof device

In this section we are going to design a plate which will be able to provide the same sensations but with a greater workspace, adapted to the amplitudes of movement in active touch condition. This plate can bend by means of PZT piezoceramics glued on one of the two surfaces. The monomorph dimensions are going to be chosen in order to satisfy ergonomic and squeeze film effect requirements. Then, we proceed to experimental verifications.

3.1 Design of the monomorph

We have at our disposal passive materials in Copper Beryllium, and a piezoelectric ceramics PZT, referred to as PI-91, marketed by Saint-Gobain Quartz company. The characteristics of the material are indicated in Table 4. The

Mechanical properties of the resonator	
Young modulus E_i $(10^9 N.m^{-2})$	123
Mechanical properties of P1-91 ceramic	
Piezoelectric constant e_{31_p} $(C.m^{-2})$	-4.9
Elastic constant $c^E_{11_p} = \frac{s^E_{11}}{(s^E_{11})^2-(s^E_{12})^2}$ $(10^{10} N.m^{-2})$	6.79
Charge coefficient d_{31} $(10^{-12} m.V^{-1})$	-247
Mechanical quality factor Q_m	60

Table 3. List of parameters

voltage supply of piezoactive ceramics is set to 15V in order to avoid a dangerous voltage. Moreover, the thickness of the piezoceramic is 1 mm, while the thickness of the substrate is set to 2 mm (this value has been chosen to guarantee mechanical holding and fabrication considerations).

3.1.1 An ergonomic workspace

The compatibility of our tactile device with the user's movement does not have to exclusively deserve the mechanisms of stimulation. It also has to offer perspectives on tangible interaction with computer-generated surfaces for example. Therefore, the definition of the ergonomic workspace plays an important role for the use of such devices. For finely textured surfaces, it is recommended to "allow the freedom of active exploration" [11]. For that purpose, the biggest exploration surface needs to be considered for the design of the tactile plate. There is no exact dimension of exploration surface in literature, but it is known, according to the observations of Klatzky and Lederman, that typically the finger quickly rubs back and forth along a small, homogeneous area of the surface, and that interior surfaces are explored rather than edges [12]. Moreover, useful information in measurements of movement amplitudes are reported in [13]. In his experiment, this author collects the position and normal force exerted by the fingertip while volunteers are actively exploring finely textured surfaces. The values for the movement amplitude along the X and Y directions are 97.27mm and

84.38mm. The mean and the biggest rectangular areas that are touched measure respectively 28.18cm^2 and 128.37 cm^2.
Within those guidelines, we can choose the width, b, of the plate in order to have a surface area higher than 28.18cm^2. Thus, we choose $b = 50mm$.

3.1.2 Squeeze film effect requirements

Now that we know the thickness and the width of the monomorph, the length has still to be found. This choice is the most important for a good working of the device because the flexural wave propagate along the length. The choice relies on a condition on the frequency and on a condition relative to coefficient of friction at the same time.

a/ Condition on the frequency

The first condition is done by the squeeze number, σ, which has to be higher than 10 as we previously mention. We calculate the squeeze number σ as shown in (4), with the parameters of Table 1 as a function of the frequency of the oscillation for a given amplitude h_{vib}. Considering the most unfavorable case, i.e. the smallest slope of the straight line representing $\sigma = f(\omega_0)$ (a surface state, h_r, of 1.6 μm and a vibration amplitude, h_{vib}, of 3μm), the results show a first criterion on the frequency (f >20.6 kHz) which enables us to use the equation (5).

Furthermore, the resonance frequency, f_n, is a function of the plate dimensions and can be expressed by the following equation:

$$f_n = \left(\frac{\pi}{\lambda/2}\right)^2 \sqrt{\frac{G_b}{M_b}} \tag{15}$$

in which M_b is the total mass per length, expressed as follow:

$$M_b = \rho_p h_p + \rho_i h_i \tag{16}$$

in which G_b is the flexional rigidity of the monomorph in N.m. G_b is the sum of the flexional rigidity of both materials where z here is measured from the neutral axis.

$$G_b = c^E_{11_p} b \int_{piezo} z^2\, dz + E_i b \int_{substrate} z^2\, dz \tag{17}$$

In Fig.10, the evolution of the resonant frequency obtained from (Eq. 15), f_n, is represented according to the half wavelength. To match the condition on the frequency according to the squeeze number, we need $f_n > 20.6kHz$, which implies that the half wavelength needs to be smaller than 16.1 mm. Thus, we obtain with this study an upper boundary for the wavelength.

b/ Condition on the relative coefficient of friction

According to the study on the stator of the PEM (Fig. 5), we need a relative coefficient of friction μ'/μ lower or equal to 0.7 in order to feel a difference of sensation. We

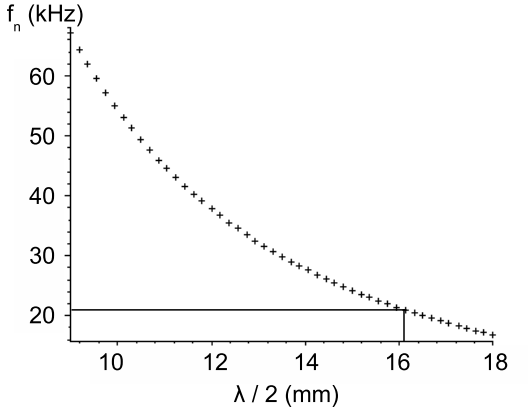

Fig. 10. Natural frequency as a function of the half wavelength.

calculate the relative coefficient of friction with the same parameters and for 4 half-wavelengths lower than 16.1 mm (Fig. 11). In this manner, we have 4 vibration amplitudes corresponding to this value. Considering the Fig.11, it is

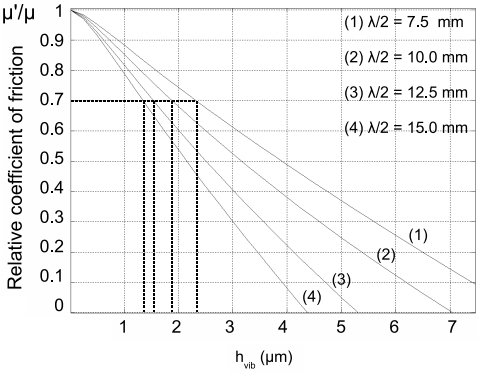

Fig. 11. The relative coefficient of friction as a function of the amplitude of vibration for $F_f = 0.5N$, $h_r = 0.6\mu m$ and for 4 values of $\lambda/2$.

necessary to obtain vibration amplitudes of 1.4, 1.55, 1.9 and 2.3μm if we choose half-wavelength of 7.5, 10, 12.5 and 15mm respectively. As we can see, a small wavelength will impose a high vibration amplitude and we will be limited quite rapidly because an vibration amplitude higher than 2μm is difficult to reach. For that aim, we choose $\lambda/2 \geq 10mm$.
Then, following the requirement for the design, we choose a surface length $\mathcal{L} = 83mm$ in order to put 7 ceramics measuring 11mm isolated from each other by a distance of 1mm. The final dimensions of the plate are: $\mathcal{L} \times b = 83mm \times 49mm$. This gives us a surface area of $40.67cm^2$.

3.1.3 Numerical study on the entire monomorph

The FE model of the monomorph is represented in Figure 12. A modal analysis is performed considering the entire

mono-morph. We find the (8; 0) mode which corresponds to a half-wavelength of $10.37mm$ in the X direction. The modal shape is presented in Fig.13 and proves that this resonance frequency (35.6kHz) is in concordance with the squeeze analysis (>20.6kHz). Afterward, we check if

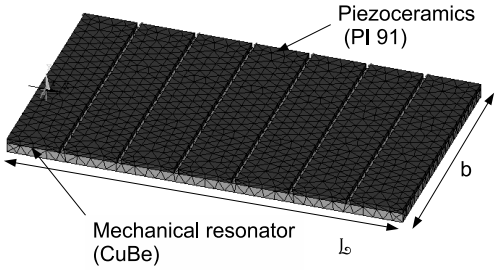

Fig. 12. FE model of the monomorph.

Fig. 13. Result of the modal analysis: deformed shape of the (8;0) mode at f=35.6kHz.

those dimensions meet amplitude requirements thanks to an harmonic analysis. The ceramics are activated by two electrical signals, with a 180^o phase shift between each which creates a standing wave (Fig. 13). The harmonic response of the actuator gives the vertical displacement as a function of the frequency (Fig.14) and shows that the natural frequency is located at 34.77kHz. With this frequency, a vertical displacement of $3.2\mu m$ is obtained at the top of the standing wave.

3.2 Experimental verifications

The prototype is presented in Fig.15. The polarity of each ceramic is oriented to satisfy the wave production along the X direction. The device is supplied by one voltage source adjusted to a mechanical resonance frequency so as to generate a standing wave along the length of the plate. Some experiments with the prototype built at the laboratory have been performed to confirm analytical and numerical studies.

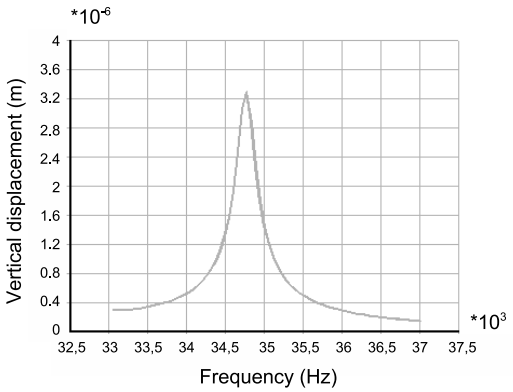

Fig. 14. Result of the harmonic analysis: Vertical displacement of a surface point.

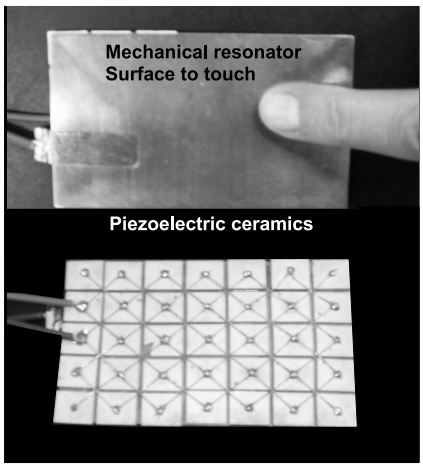

Fig. 15. Complete view of the actuator: below side with a piezo-ceramics matrix and above side which is the surface to touch.

3.2.1 Vibration amplitude measurement

The vibration amplitude is measured using a single-point LASER Doppler Vibrometer (OFV505) linked to a controller (OFV-5000) that is connected to an oscilloscope.

As the results show, a deflection amplitude of about $2.3\mu m$ peak to peak is obtained by applying a voltage of 15V. The resonant frequency is 30.5kHz, which gives a squeeze number of 15.9 for $h_r = 0.6\mu m$.

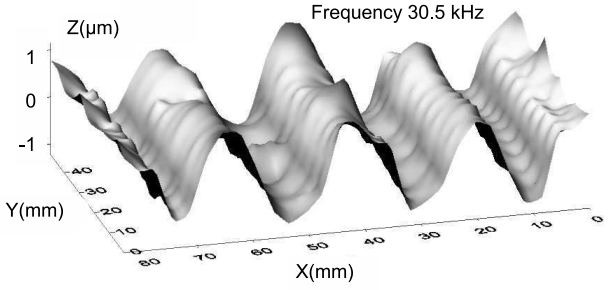

Fig. 16. Laser vibrometric measurements of the (8; 0) mode.

The vibration amplitude of the prototype is smaller than the predicted amplitude. This amplitude attenuation may be due to the manufacturing of the monomorph and especially to the gluing phase. More precisely, the gluing phase is crucial for the vibration quality owing to the ideal gluing hypothesis. However, according to the relative friction study, this vibration amplitude of the plate can be enough to feel the difference of perception. This assumption will be checked in the next section.

3.2.2 Qualitative study of the sensation

Space period of the gratings	**Space period simulated**				
	0.4 *mm*	2 *mm*	4 *mm*	8 *mm*	10 *mm*
0.4 *mm*					
2 *mm*					
4 *mm*					
8 *mm*					
10 *mm*					

Table 4. Percentage of answer

4 Conclusion

This paper described a new, modular, high-performance, tactile transducer device based on the squeeze film effect principle. It had 60 actuators creating an active surface of about 10 mm2 in the shape of a cradle designed to minimize the finger pre-load when the tactile signals is quiescent. The system is compact (150 cm2, 60 g) and has integrated electronics requiring a small number of connection wires for operation. A prominent feature the device is the ease with which is can be fabricated and serviced. The results indicated that each actuator could produce a free deflection of 0.1 mm and a blocked force of 0.15 N (or 0.075 mm and

In this article, we have presented a complete modeling of a planar standing wave ultrasonic motor. Firstly, the vibratory behavior has been analytically introduced with the variational formulation. Then, an experimental iden- tication method is presented and allows to identify some nonlinearities of the freely vibrating plate. The experi- mental results are compared to the analytical ones. This approach is validated for a single vibratory mode, but may be extended for all others, indiscriminately along the length or width of the plate. Secondly, the mechanical conversion is introduced. This part of modeling is at the origin of important non-linearities because of mechanical asymmetry, possibly increased by the intermittent contact phenomenon. Nevertheless, the overall behavior can be expressed from simple relations, since the inertia of the actuator lters the small vibratory transitions of the contact. By this way, an average modeling of the tangential motion is established. The tangential results are strongly dependent on the motion along the normal axis, mainly induced by the intermittent contact. This inter- mittent contact varies according to the normal pre-load or also with the wave amplitude. Some experimental mea- surements were sucient to emphasize the overall behav- ior and validate the simplied mechanical approach. At last, the complete identied modelling is discussed, thanks to causal ordering graph formalism. It will be useful for deducing a force control law, as presented in [?].

References

1. A. Talbi, O. Ducloux, N. Tiercelin, Y. Deblock, P. Pernod, V. Preobrazhensky. Vibrotactile using micromachined electromagnetic actuators array. *Journal of Physics: Conference Series. International MEMS Conference*, 34:637–642, 2006.
2. T. Watanabe, S. Fukui. A method for controlling tactile sensation of surface roughness using ultrasonic vibration. *IEEE Int. Conf. on Robotics and Automation*, pages 1134–1139, 1995.
3. J. Loomis, S. J. Lederman. *Tactual perception.* K. Boff, L. Kaufman and J. Thomas Eds. Handbook of Perception and Human Performance, New York: John Wiley & Sons.
4. E.O.J. Salbu. Compressible squeeze films and squeeze bearings. *ASME J. Basic Engng*, 86:355–366, 1964.
5. M. Wiesendanger. *Squeeze Film air Bearings Using Piezoelectric Bending Elements.* PhD thesis, EPFL, Switzerland, 2000.
6. T. Maeno, K. Kobayashi, N. Yamazaki. Relationship between the structure of human finger tissue and the location of tactile receptors. *Bulletin of JSME International Journal*, 41.
7. A. M. Smith, G. Gosselin, B. Houde. Deployment of fingertip forces in tactile exploration. *Experimental brain research*, 147:209–218, september 2002.
8. T. Maeno, D. B. Bogy. Effect of the hydrodynamic bearing on rotor/stator contact in a ring-type ultrasonic motor. *IEEE Transations on Ultrasonics, Ferroelectrics, and Frequency Control*, 39:675–682, november 1992.
9. M. Biet, L. Boulon, F. Martinot, F. Giraud, B. Semail. Using an ultrasonic transducer: Evidence for an anisotropic deprivation of frictional cues in microtexture perception. *To appear in IEEE WorldHaptics*, March 2007.
10. F. Martinot, A. Houzefa, M. Biet, C. Chaillou. Mechanical responses of the fingerpad and distal phalanx to friction of a grooved surface: Effect of the contact angle. *14th Symposium on Haptic Interfaces for Virtual Environment and Teleoperator Systems*, pages 297–300.
11. J. Pasquero, V. Hayward. Stress: A practical tactile display system with one millimeter spatial resolution and 700 hz refresh rate. *In Eurohaptics Proceeding, Dublin*, 2003.
12. S. J. Lederman, R. L. Klatzky. Hand movements : a window into haptic object recognition. *Cognitive psychology*, 19:342–368, 1987.
13. F. Martinot. *Caractérisation du rôle de la dynamique du toucher dans la perception de textures.* PhD thesis, USTL Lille; France, 2006.